Extension of the binary-encounter-dipole model to relativistic incident electrons

Yong-Ki Kim
National Institute of Standards and Technology, Gaithersburg, Maryland 20899-8423

José Paulo Santos
Departamento de Física, Faculdade de Ciências e Tecnologia, Universidade Nova de Lisboa, Monte de Caparica, 2825-114 Caparica, Portugal
and Centro de Física Atómica da Universidade de Lisboa, Avenida Professor Gama Pinto 2, 1649-003 Lisboa, Portugal

Fernando Parente
Departamento Física da Universidade de Lisboa and Centro de Física Atómica da Universidade de Lisboa, Avenida Professor Gama Pinto 2, 1649-003 Lisboa, Portugal
(Received 18 May 2000; published 13 October 2000)

Formulas for the total ionization cross section by electron impact based on the binary-encounter-dipole (BED) model and its simpler version, the binary-encounter-Bethe (BEB) model are extended to relativistic incident electron energies. Total ionization cross sections for the hydrogen and helium atoms from the new relativistic formulas are compared to experimental data. Relativistic effects double the total ionization cross section of H and He at incident electron energy ≈ 300 keV and dominate the cross section thereafter. A simple modification of the original BED-BEB formulas is proposed for applications to ion targets and inner-shell electrons of neutral atoms and molecules. The relativistic and nonrelativistic BEB cross sections are compared to the *K*-shell ionization cross sections by electron impact for the carbon, argon, nickel, niobium, and silver atoms. For carbon and argon, the relativistic effects are small, and both forms of the BEB cross sections agree well with available experimental data. For the nickel and heavier atoms, the relativistic increase of cross sections becomes noticeable from about 100 keV and higher in the incident electron energy. The empirical formula by Casnati *et al.* [J. Phys. B **15**, 155 (1982)] after correcting for relativistic effects as shown by Quarles [Phys. Rev. A **13**, 1278 (1976)] agrees well with the BEB cross sections for light atoms. However, the peak values of the Casnati cross sections become higher than the relativistic BEB peak cross sections as the atomic number increases. The BEB model is also applied to the total ionization cross section of the xenon atom, and the theory agrees well with experiments at low incident electron energies, but disagrees with experiment at relativistic incident energies.

PACS number(s): 34.80.Dp, 34.80.Gs, 34.80.Kw

I. INTRODUCTION

In an earlier work Kim and Rudd [1] proposed the binary-encounter-dipole (BED) model for the singly differential (energy distribution of secondary electrons) ionization cross section $d\sigma/dW$ as a function of the secondary electron energy W and the incident electron energy T. The total ionization cross section is obtained by integrating over W. In this paper the nonrelativistic BED and associated formulas for the singly differential and total ionization cross sections are extended to relativistic incident electrons. The relativistic forms are required when T exceeds about 20 keV, e.g., in the inner-shell ionization of heavy atoms by fast electrons and the stripping of fast ions used in heavy ion fusion.

The BED model was developed by combining a modified form of the Mott cross section [2,3] and the leading dipole part of the Bethe cross section [4]. The relativistic extension of the Mott cross section, which is known as the Møller cross section [5], and that for the Bethe cross section are different, and we must go back to the differential ionization cross section and identify the origin of various terms to apply the correct relativistic extensions.

The BED model requires the knowledge of differential dipole oscillator strength, df/dW, for each atomic or molecular orbital. When df/dW is unknown, Kim and Rudd approximate it by a simple analytic function and obtain a compact, analytic expression for the total ionization cross section. This simplified version is referred to as the binary-encounter-Bethe (BEB) model [1]. The BED-BEB model was used to calculate total ionization cross sections of neutral atoms and molecules with great success [6] for nonrelativistic incident electron energies.

In Sec. II we summarize the nonrelativistic BED-BEB formulas and identify changes necessary to transform them into relativistic forms. In Sec. III we discuss the application of the relativistic formulas. One class of problems to which the present relativistic formulas are immediately applicable is *K*-shell ionization cross sections. The original BED-BEB model is designed to produce reliable cross sections for neutral targets. To extend the model to inner-shell ionization, the BED-BEB model is modified slightly to account for the strong nuclear field experienced by the incident electron when colliding with inner-shell electrons. Conclusions are presented in Sec. IV.

II. THEORY

The BED-BEB cross-section formulas for atomic and molecular targets are identical. We shall refer to atoms for brev-

ity hereafter, with the understanding that the same formulas can also be applied to molecular targets.

A. Nonrelativistic formula for differential ionization cross sections

The modified Mott cross section used in the BED model for the differential ionization cross section per atomic orbital is [1]

$$\left(\frac{d\sigma}{dW}\right)_{\text{Mott}}=\frac{4\pi a_0^2R^2N}{T}\left[\frac{1}{(W+B)^2}-\frac{1}{(W+B)(T-W)}+\frac{1}{(T-W)^2}\right], \tag{1}$$

where T is the incident electron energy, W is the kinetic energy of the ejected electron, B is the orbital binding energy, R is the Rydberg energy ($=13.6$ eV), N is the orbital electron occupation number, and $a_0(=0.529$ Å) is the Bohr radius.

Since the Mott cross section does not include the dipole interaction, i.e., the soft collision with small momentum transfers characteristic of bound electrons, the modified Mott cross section, Eq. (1), is combined with the leading dipole term of the Bethe cross section to obtain the BED formula. The original Mott cross section was derived using the Coulomb functions for two free, colliding electrons, while the Bethe cross section, which is the asymptotic (high T) form of the plane-wave Born approximation, used plane waves for the incident and scattered electrons. Hence, the two formulas cannot simply be added.

The differential Bethe cross section is often given in the form [7,8]:

$$\left(\frac{d\sigma}{dW}\right)_{\text{Bethe}}=\frac{4\pi a_0^2}{T}[A(W/R)\ln(T/R)+C(W/R)+\cdots], \tag{2}$$

where $A(W/R)$ and $C(W/R)$ are functions characteristic of the target atom but independent of T.

Many past attempts to combine the Mott cross section with the Bethe cross section involved adjustable (mostly empirical) parameters to scale the Bethe or Mott cross section. Instead, Kim and Rudd required the combined formulas to satisfy asymptotic forms for both the ionization cross section and the stopping cross section [4,7], and succeeded in eliminating any adjustable parameters. In addition, in the BED model the first denominator T on the right-hand side (RHS) of Eqs. (1) and (2) was replaced by $T+U+B$, where $U=\langle \boldsymbol{p}^2/2m\rangle$ is the average orbital kinetic energy of the target electron, $\boldsymbol{p}$ being the electron momentum and m the electron rest mass. This replacement was introduced by Burgess [9] to emulate the correlation between incident and the target electrons. The nonrelativistic BED model for neutral targets significantly owes its success at low T to the use of this denominator, which is sometimes referred to as the ''focusing term'' or the ''acceleration term.'' This means that the incident electron is attracted by the target nucleus and gains speed before collision. In reality, the incident electron sees a neutral target until it actually plows into the target charge cloud. The replacement of the denominator introduced by Burgess [9] is a simple yet effective way to have a mildly T-dependent correlation term between the incident and target electrons.

With these modifications, the nonrelativistic BED formula for the singly differential ionization cross section per atomic or molecular orbital is given by [1]

$$\left(\frac{d\sigma}{dW}\right)_{\text{BED}}=\frac{S}{B(t+u+1)}\left\{\frac{(N_i/N)-2}{t+1}\left(\frac{1}{w+1}+\frac{1}{t-w}\right)+[2-(N_i/N)]\left[\frac{1}{(w+1)^2}+\frac{1}{(t-w)^2}\right]+\frac{\ln t}{N(w+1)}\frac{df}{dw}\right\}, \tag{3}$$

where $S=4\pi a_0^2N(R/B)^2$, $t=T/B$, $u=U/B$, $w=W/B$, and

$$N_i=\int_0^\infty (df/dw)dw, \tag{4}$$

in terms of the differential dipole oscillator strength df/dw, which uses the binding energy as the energy interval.

In Eq. (3) the first two terms in the curly brackets on the RHS associated with the factor $\pm(2-N_i/N)$ are from the Mott cross section, Eq. (1), while the last term with df/dw is the leading dipole term from the Bethe cross section, Eq. (2). As is shown later, the changes necessary for relativistic T must be introduced in the differential ionization cross section.

B. Nonrelativistic formulas for total ionization cross sections

To obtain the nonrelativistic BED cross section σ_{BED} for total ionization, we integrate Eq. (3) over the secondary electron energy, $W=0$ to $W_{max}=(T-B)/2$, and get the total ionization cross section:

$$\sigma_{\text{BED}}=\frac{S}{t+u+1}\left[D(t)\ln t+\left(2-\frac{N_i}{N}\right)\left(1-\frac{1}{t}-\frac{\ln t}{t+1}\right)\right], \tag{5}$$

where

$$D(t)\equiv N^{-1}\int_0^{(t-1)/2}\frac{1}{w+1}\frac{df(w)}{dw}dw \tag{6}$$

and N_i is defined by Eq. (4).

Often it is difficult to find reliable df/dw for individual atomic or molecular orbitals. In such cases, Kim and Rudd [1] approximate the differential dipole oscillator strength for all orbitals by a simple function that simulates the shape of the df/dw for ionizing the hydrogen atom,

$$\left(\frac{df}{dw}\right)_{\mathrm{BEQ}}=\frac{N_i}{(w+1)^2}. \tag{7}$$

This simplification is referred to as the BEQ model. Since the dipole term in Eq. (3) with Eq. (7) becomes proportional to $1/(w+1)^3$, we also symmetrize the dipole term following the symmetric form of the Mott cross section in the same equation, i.e., $(df/dw)/(w+1)$ in Eq. (3) is replaced by $N_i[1/(w+1)^3+1/(t-w)^3]$ before the differential cross section is integrated over w. Then the integrated cross section per orbital in the BEQ model becomes a simple analytic formula,

$$\sigma_{\mathrm{BEQ}}=\frac{S}{t+u+1}\left[\frac{Q\ln t}{2}\left(1-\frac{1}{t^2}\right)+(2-Q)\left(1-\frac{1}{t}-\frac{\ln t}{t+1}\right)\right] \tag{8}$$

in terms of a dipole constant Q defined in the derivation of Eq. (3),

$$Q=\frac{2BM^2}{NR}, \tag{9}$$

with a frequently used dipole constant M^2 defined by

$$M^2=\frac{R}{B}\int_0^\infty \frac{1}{w+1}\frac{df}{dw}dw\equiv ND(\infty). \tag{10}$$

Note that the first logarithmic term on the RHS of Eq. (8) represents the dipole term, the middle term $(1-1/t)$ embodies the direct and exchange contributions from the Mott cross section, and the last logarithmic term originates from the interference between the direct and exchange contributions. Equation (8) requires only four constants from each atomic or molecular orbital, viz., the binding energy B, the kinetic energy U, the electron occupation number N, all from the ground-state wave function of the target, and the dipole constant Q. The substitution of Eq. (7) into Eq. (10) leads to $Q_{\mathrm{BEQ}}=N_i/N$, which is used to replace N_i/N when Eq. (3) is integrated.

When a reliable value of M^2 is known, although the details of df/dw are unknown, the M^2 value can be used to determine Q via Eq. (9). This substitution will make σ_{BEQ} converge to the correct asymptotic limit predicted by the Bethe theory.

When no data are available either for df/dw or Q, Kim and Rudd [1] set $Q=1$, which they called the binary-encounter-Bethe (BEB) model. Then, the BEB cross section becomes very simple,

$$\sigma_{\mathrm{BEB}}=\frac{S}{t+u+1}\left[\frac{\ln t}{2}\left(1-\frac{1}{t^2}\right)+1-\frac{1}{t}-\frac{\ln t}{t+1}\right]. \tag{11}$$

C. Relativistic BED, BEQ, and BEB cross sections

The original Mott and the Bethe cross sections have started with momentum transfers, and the expressions in terms of energy, such as T and W, have been obtained by converting relevant electron speed into energies using the nonrelativistic relation. For instance, a kinetic energy K is obtained by setting $K=mv^2/2$, where v is the speed of an electron. The relativistic formulas, on the other hand, are written in terms of the ratio of the electron speed to the speed of light c,

$$\beta_t=v_t/c,\quad \beta_t^2=1-\frac{1}{(1+t')^2},\quad t'=T/mc^2, \tag{12}$$

$$\beta_b=v_b/c,\quad \beta_b^2=1-\frac{1}{(1+b')^2},\quad b'=B/mc^2, \tag{13}$$

and

$$\beta_u=v_u/c,\quad \beta_u^2=1-\frac{1}{(1+u')^2},\quad u'=U/mc^2, \tag{14}$$

where v_t is the speed of an electron with kinetic energy T, v_b is the speed of an electron with kinetic energy B, and v_u is the speed of an electron with kinetic energy U.

The Møller cross section per atomic orbital, after the same modification used on the original Mott cross section to avoid singularities for $W=0$ and multiplying the orbital electron occupation number N, is given by [10–12]

$$\left(\frac{d\sigma}{dw}\right)_{\mathrm{Møller}}=\frac{4\pi a_0^2\alpha^2N(R/B)}{\beta_t^2}\left[\frac{1}{(w+1)^2}+\frac{1}{(t-w)^2}+\frac{b'^2}{(1+t')^2}-\frac{1}{(w+1)(t-w)}\frac{1+2t'}{(1+t')^2}\right], \tag{15}$$

where α is the fine-structure constant. The integration of the differential Møller cross section from $w=0$ to $w_{max}=(t-1)/2$ results in the integrated Møller cross section,

$$\sigma_{\mathrm{Møller}}=\frac{4\pi a_0^2\alpha^2N(R/B)}{\beta_t^2}\left[1-\frac{1}{t}-\frac{\ln t}{t+1}\frac{1+2t'}{(1+t')^2}+\frac{b'^2}{(1+t')^2}\frac{t-1}{2}\right]. \tag{16}$$

The relativistic form of the nonrelativistic Bethe cross section, Eq. (2), is [7,8,11–13]

$$\frac{d\sigma}{d(W/R)}=\frac{4\pi a_0^2\alpha^2}{\beta_t^2}\left\{A(W/R)\left[\ln\left(\frac{\beta_t^2}{1-\beta_t^2}\right)-\beta_t^2\right]+C'(W/R)+\cdots\right\}, \tag{17}$$

where

$$C'(W/R)=C(W/R)-2A(W/R)\ln\alpha. \tag{18}$$

The nonrelativistic Eq. (3) is converted to a relativistic form to match the relativistic Eqs. (15) and (17), while noting that Eqs. (2) and (3) use different energy units in the logarithm associated with the dipole interaction. After replacing β_t^2 in the first denominator on the RHS of Eqs. (16) and (17) by the relativistic equivalent of the ''Burgess'' denominator, $\beta_t^2+\beta_u^2+\beta_b^2$, the relativistic BED (RBED) formula for the singly differential ionization cross section becomes

$$\left(\frac{d\sigma}{dW}\right)_{\mathrm{RBED}}=\frac{4\pi a_0^2\alpha^4 N}{(\beta_t^2+\beta_u^2+\beta_b^2)2b'}\left\{\frac{(N_i/N)-2}{t+1}\left(\frac{1}{w+1}+\frac{1}{t-w}\right)\frac{1+2t'}{(1+t'/2)^2}\right.$$
$$+[2-(N_i/N)]\left[\frac{1}{(w+1)^2}+\frac{1}{(t-w)^2}+\frac{b'^2}{(1+t'/2)^2}\right]$$
$$\left.+\frac{1}{N(w+1)}\frac{df}{dw}\left[\ln\left(\frac{\beta_t^2}{1-\beta_t^2}\right)-\beta_t^2-\ln(2b')\right]\right\}. \tag{19}$$

The total ionization cross section of an atomic orbital is obtained by integrating Eq. (19) over w from 0 to $(t-1)/2$,

$$\sigma_{\mathrm{RBED}}=\frac{4\pi a_0^2\alpha^4 N}{(\beta_t^2+\beta_u^2+\beta_b^2)2b'}\left\{D(t)\left[\ln\left(\frac{\beta_t^2}{1-\beta_t^2}\right)-\beta_t^2-\ln(2b')\right]+\left(2-\frac{N_i}{N}\right)\left[1-\frac{1}{t}-\frac{\ln t}{t+1}\frac{1+2t'}{(1+t'/2)^2}+\frac{b'^2}{(1+t'/2)^2}\frac{t-1}{2}\right]\right\}, \tag{20}$$

while $D(t)$ is given by Eq. (6).

The matching relativistic BEQ (RBEQ) and relativistic BEB (RBEB) formulas for total ionization of an atomic or molecular orbital are

$$\sigma_{\mathrm{RBEQ}}=\frac{4\pi a_0^2\alpha^4 N}{(\beta_t^2+\beta_u^2+\beta_b^2)2b'}\left\{\frac{Q}{2}\left[\ln\left(\frac{\beta_t^2}{1-\beta_t^2}\right)-\beta_t^2-\ln(2b')\right]\left(1-\frac{1}{t^2}\right)\right.$$
$$\left.+(2-Q)\left[1-\frac{1}{t}-\frac{\ln t}{t+1}\frac{1+2t'}{(1+t'/2)^2}+\frac{b'^2}{(1+t'/2)^2}\frac{t-1}{2}\right]\right\}, \tag{21}$$

and

$$\sigma_{\mathrm{RBEB}}=\frac{4\pi a_0^2\alpha^4 N}{(\beta_t^2+\beta_u^2+\beta_b^2)2b'}\left\{\frac{1}{2}\left[\ln\left(\frac{\beta_t^2}{1-\beta_t^2}\right)-\beta_t^2-\ln(2b')\right]\left(1-\frac{1}{t^2}\right)+1-\frac{1}{t}-\frac{\ln t}{t+1}\frac{1+2t'}{(1+t'/2)^2}+\frac{b'^2}{(1+t'/2)^2}\frac{t-1}{2}\right\}. \tag{22}$$

The relativistic Eqs. (20)–(22) reduce to their nonrelativistic counterparts, Eqs. (5), (8), and (11) in the limit $\beta_t\ll 1$ by noting that $R=mc^2\alpha^2/2$, $mv_t^2/2\cong T$, $mv_u^2/2\cong U$, and $mv_b^2/2\cong B$.

D. Asymptotic limits

The Bethe cross section for the total ionization in the high-T limit is often given by two constants M^2 and C, which are characteristic of the target but independent of T [7],

$$\sigma_{\mathrm{RBethe}}=\frac{4\pi a_0^2\alpha^2}{\beta_t^2}\left\{M^2\left[\ln\left(\frac{\beta_t^2}{1-\beta_t^2}\right)-\beta_t^2\right]+C_R\right\} \tag{23}$$

in the relativistic form, and

$$\sigma_{\mathrm{NRBethe}}=\frac{4\pi a_0^2}{T/R}\left[M^2\ln\frac{T}{R}+C_{NR}\right] \tag{24}$$

in the nonrelativistic form. The quantity C_R is related to C_{NR} by Eq. (18), i.e.,

$$C_R = C_{NR} - 2M^2 \ln \alpha. \tag{25}$$

Since the BED-BEQ-BEB cross sections are given in analytic forms, we can easily obtain analytic expressions for M^2 and C from these cross-section models. The expression for M^2 is the same for relativistic and nonrelativistic formulas. The nonrelativistic expressions are

$$M^2_{\mathrm{BED}} = \frac{NR}{B} D(\infty), \tag{26}$$

$$C_{\mathrm{NRBED}} = M^2_{\mathrm{BED}} \ln\left(\frac{R}{B}\right) + \frac{NR}{B}\left(2 - \frac{N_i}{N}\right); \tag{27}$$

$$M^2_{\mathrm{BEQ}} = \frac{NRQ}{2B}, \tag{28}$$

$$C_{\mathrm{NRBEQ}} = M^2_{\mathrm{BEQ}} \ln\left(\frac{R}{B}\right) + \frac{NR}{B}(2 - Q); \tag{29}$$

$$M^2_{\mathrm{BEB}} = \frac{NR}{2B}, \tag{30}$$

$$C_{\mathrm{NRBEB}} = M^2_{\mathrm{BEB}} \ln\left(\frac{R}{B}\right) + \frac{NR}{B}; \tag{31}$$

and the relativistic expressions for C can be derived using Eq. (25).

As was mentioned earlier, M^2_{BED} is a weighted integral of the differential dipole oscillator strength, Eqs. (6) and (10), and can be determined if df/dw for all orbitals are known, either from photoionization experiments or a reliable theory. For instance, the values of M^2 are known for H and H-like ions, He and some He-like ions, Ne, Ar, Kr, and Xe [14]. The second constant, C_{NR}, is much more difficult to determine, and reliable values are known only for a short list of targets. The M^2 from the BED and BEQ formulas are identical to those from the Bethe theory, but M^2_{BEB} is not, because of the approximation $Q=1$ we have made to obtain σ_{BEB}. None of the C values from the present models are the same as the Bethe theory value because of the approximations we have made to combine the Bethe and Mott cross sections. For very high $T \gg mc^2$, the approximations we have made, while providing reliable cross sections at $T<5$ keV, may lead to less reliable cross sections than accurate asymptotic Bethe cross sections when they are known.

III. APPLICATION OF THE RELATIVISTIC FORMULAS

Cross-section formulas based solely on the Bethe theory are reliable for high T but are usually unreliable at low T where the ionization cross sections peak. Since the nonrelativistic BED-BEB formulas provide reliable ionization cross sections at low T and the relativistic BED-BEB formulas reduce to the correct nonrelativistic BED-BEB formulas, the relativistic BED-BEB cross sections should provide reliable ionization cross sections for a wide range of T. For instance, Eq. (22) is ideally suited for modeling ionizing events that cover incident electron energies from the threshold to hundreds of keV because the BEB model requires minimal input data for the target.

Note that the ''Burgess'' denominator, $T+U+B$, is the only *ad hoc* term used without proper derivation in the BED model. The substantial reduction of cross sections at low T achieved by the Burgess denominator for neutral targets is unlikely to be correct in magnitude when the incident electron is subject to a long-range Coulomb interaction from an ion target. Kim and Rudd [1] already noted that they had to reduce the denominator to apply the nonrelativistic BED model to He^+. Further application of the BEB model to singly charged molecular ions [15] revealed that using $T+(U+B)/2$ instead of $T+U+B$ resulted in excellent agreement with known experimental data at nonrelativistic T.

Moreover, comparisons to distorted-wave Born cross sections for highly charged ions [16] indicate that a simple average of the nonrelativistic BED, BEQ, and BEB cross sections with the $t+u+1$ denominator and t reproduces the distorted-wave Born results closely at low to intermediate t. For extreme cases such as the hydrogenic ions of heavy atoms, we expect that t alone will be the appropriate denominator as is the case for most *ab initio* theories that are expected to be valid for such targets.

Until we have more examples to compare, we *tentatively* propose to use *for single ionization of deep inner shells* of heavy atoms,

$$\sigma_{\mathrm{BEDav}} = \frac{S}{2}\left(\frac{1}{t} + \frac{1}{t+u+1}\right) \times \left[D(t)\ln t + \left(2 - \frac{N_i}{N}\right)\left(\frac{t-1}{t} - \frac{\ln t}{t+1}\right)\right] \tag{32}$$

instead of Eq. (5),

$$\sigma_{\mathrm{BEQav}} = \frac{S}{2}\left(\frac{1}{t} + \frac{1}{t+u+1}\right)\left[\frac{Q\ln t}{2}\left(1 - \frac{1}{t^2}\right) + (2-Q)\left(1 - \frac{1}{t} - \frac{\ln t}{t+1}\right)\right] \tag{33}$$

instead of Eq. (8), and

$$\sigma_{\mathrm{BEBav}} = \frac{S}{2}\left(\frac{1}{t} + \frac{1}{t+u+1}\right)\left[\frac{\ln t}{2}\left(1 - \frac{1}{t^2}\right) + 1 - \frac{1}{t} - \frac{\ln t}{t+1}\right] \tag{34}$$

instead of Eq. (11). In fact, these averaged BED, BEQ, and BEB formulas can also be used for any ions whose net charge is $3+$ or higher, including deep inner shells which are subject to strong effective nuclear attraction. Similar to Eqs. (32)–(34), the averaged relativistic BED, BEB, and BEQ formulas are

$$\sigma_{\mathrm{RBEDav}} = \frac{1}{2}\left(1 + \frac{\beta_t^2 + \beta_u^2 + \beta_b^2}{\beta_t^2}\right) \times [\text{RHS of Eq. (20)}], \tag{35}$$

TABLE I. *K*-shell binding energy *B* [18] and kinetic energy *U*.

Element	*B*(keV)	*U*(keV)
C	0.2844	0.4372
Ar	3.203	4.228
Ni	8.331	10.521
Nb	18.983	23.363
Ag	25.516	31.268

$$\sigma_{\mathrm{RBEQav}}=\frac{1}{2}\left(1+\frac{\beta_t^2+\beta_u^2+\beta_b^2}{\beta_t^2}\right)\times[\text{RHS of Eq. (21)}], \tag{36}$$

and

$$\sigma_{\mathrm{RBEBav}}=\frac{1}{2}\left(1+\frac{\beta_t^2+\beta_u^2+\beta_b^2}{\beta_t^2}\right)\times[\text{RHS of Eq. (22)}]. \tag{37}$$

As is shown later, relativistic effects raise the ionization cross section at high $T>mc^2$, sometimes making the cross section higher than the first peak at lower *T*. This is known as the relativistic rise of ionization cross sections. When $T\gg mc^2$, other relativistic effects, such as the density effect, which is an apparent increase in the target density because of the Lorentz contraction of the length in the direction of the incident electron beam, must be taken into account.

A. Application of the BEB model to *K*-shell ionization

Inner-shell ionization cross sections by electron impact are of interest not only to the basic collision physics for complex atoms and molecules, but also to various practical applications in material science and electron microscopy. A comprehensive review of the theoretical and experimental situation as of mid-1980s has been presented by Powell [17]. Theoretical difficulties in the past were between the threshold and the peak, which occurs usually four to five times the threshold energy. Theories based on the Bethe or Born cross section are not reliable there. Theories based on classical mechanics are somewhat better but such theories usually require adjustable parameters. The present BEB-RBEB models produce reliable cross sections between the threshold and the peak without using any adjustable parameters.

As an illustration, we apply the relativistic and nonrelativistic averaged BEB formulas to the *K*-shell ionization of C, Ar, Ni, Nb, and Ag. As is shown below, relativistic effects become increasingly more important as the *K*-shell binding energies of the elements increase. Hence relativistic theory must be used for treating both atomic structure and collision dynamics for medium to heavy atoms. The only input data needed for each element in the present BEB-RBEB model are *B* and *U*, which are calculated from Dirac-Fock wave functions and listed in Table I, and the electron occupation number $N=2$. For the binding energies of inner-shell electrons, experimental values [18] may be used to match experimental thresholds precisely, though theoretical *K*-shell binding energies from Dirac-Fock wave functions are reliable to 1% or better in general.

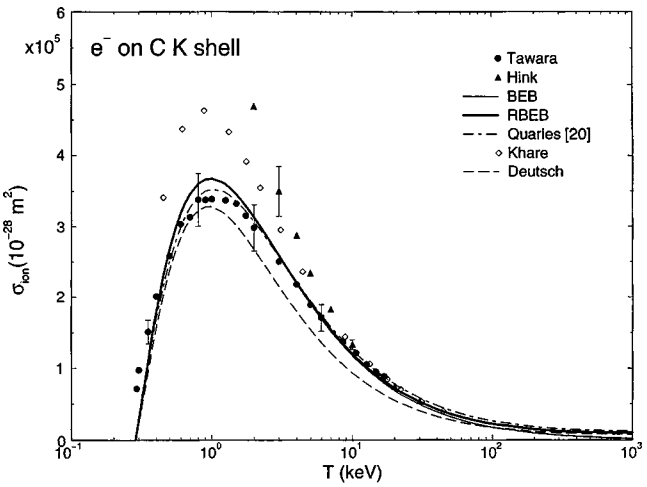

FIG. 1. *K*-shell ionization cross section of C. Solid circles, experimental data by Tawara *et al.* [25]; solid triangles, data by Hink and Paschke [26]; thin solid curve, present averaged BEB cross section, Eq. (34); thick solid curve, present averaged RBEB cross section, Eq. (37); dot-dashed curve, relativistic empirical formula by Quarles [20]; open diamonds, nonrelativistic semiempirical formula by Khare *et al.* [23]; long-dashed curve, nonrelativistic semiempirical formula by Deutsch *et al.* [22].

Before we present the comparison between theories and experiments, a few general comments are in order.

(a) Casnati *et al.* [19] determined their empirical formula by fitting to a wide range of experimental data available to them. Hence, when particular experimental data published before Casnati *et al.* agree well with the Casnati formula, the agreement may simply indicate that Casnati *et al.* gave a high weight to the experimental data while fitting their formula.

(b) Casnati *et al.* [19] presented a formula for relativistic corrections in their paper but the formula—an equation given at the end of their Sec. 3—is wrong. The correct formula is given by Quarles [20]. Hence, we quote the Casnati formula with the correct relativistic correction as the ''Quarles'' cross section, while the nonrelativistic version is called the ''Casnati'' cross section.

(c) The fitting formula developed by Casnati *et al.* [Eq. (8) in [19]] contains the leading dipole interaction terms represented by $\ln t/t$, while the relativistic correction presented by Quarles is based on the classical theory by Gryzinski [21], which does not include any dipole interaction. In contrast, the present RBEB model contains the leading dipole interaction and uses the correct relativistic extension of the dipole interaction.

(d) The semiempirical formula by Deutsch *et al.* [22] is a modified form of the classical theory by Gryzinski [21]. The modification involves introducing a new parameter and adjusting all parameters to fit available experimental data. Their formula still lacks the dipole interaction which becomes dominant at high *T*, and hence tends to be too low at relativistic *T*.

In Figs. 1–5, we compare the present BEB [Eq. (34)] and

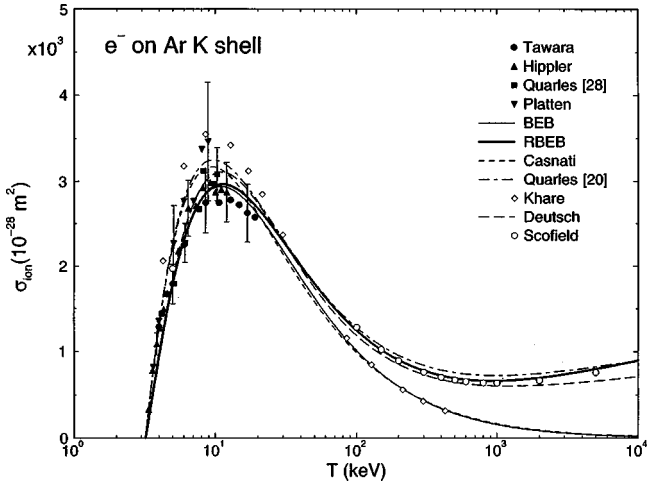

FIG. 2. *K*-shell ionization cross section of Ar. Solid circles, experimental data by Tawara *et al.* [25]; upright triangles, data by Hippler *et al.* [27]; squares, data by Quarles and Semaan [28]; inverted triangles, data by Platten *et al.* [29]; thin solid curve, present BEB cross section, Eq. (34); thick solid curve, present RBEB cross section, Eq. (37); short-dashed curve, nonrelativistic empirical formula by Casnati *et al.* [19]; dot-dashed curve, the Casnati cross section with relativistic corrections by Quarles [20]; open diamonds, nonrelativistic semiempirical formula by Khare *et al.* [23]; long-dashed curve, relativistic semiempirical formula by Deutsch *et al.* [22]; open circles, relativistic plane-wave Born cross sections by Scofield [24].

RBEB [Eq. (37)] cross sections to available experimental data, to the nonrelativistic empirical cross sections by Casnati *et al.* [19], to the relativistic version of the Casnati cross sections with the relativistic corrections provided by Quarles [20] based on Gryzinski's classical theory [21], to the nonrelativistic semiempirical cross sections by Khare *et al.* [23], to the semiempirical cross sections by Deutsch *et al.* [22],

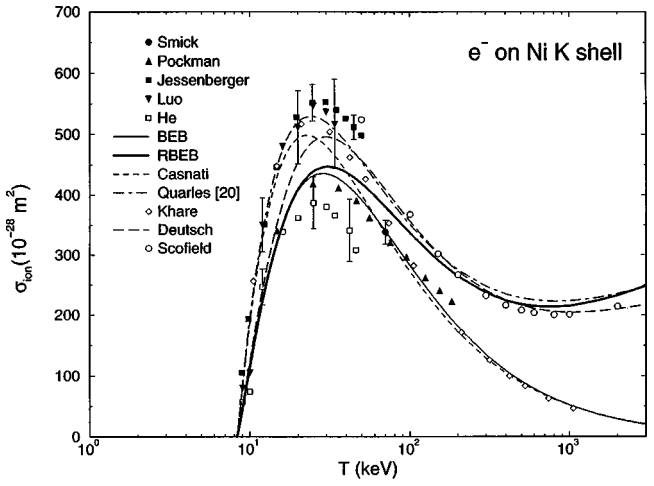

FIG. 3. *K*-shell ionization cross section of Ni. Circles, experimental data by Smick and Kirkpatrick [34]; upright triangles, data by Pockman *et al.* [33]; squares, experimental data by Jessenberger *et al.* [30]; inverted triangles, experimental data by Luo *et al.* [31]; open squares, experimental data by He *et al.* [32]; for other legends, see Fig. 2 caption.

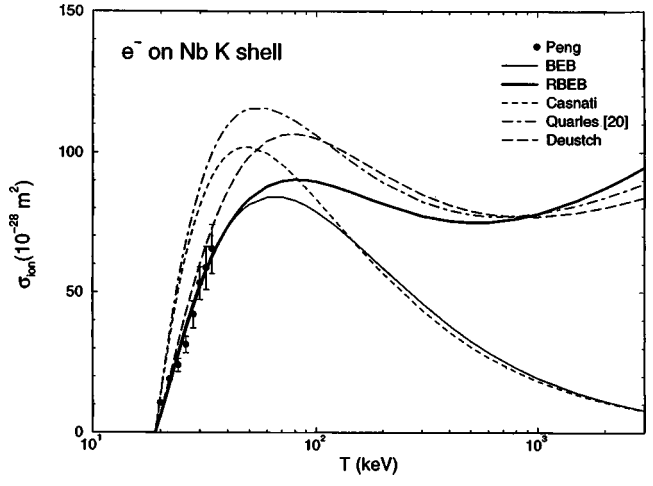

FIG. 4. *K*-shell ionization cross section of Nb. Solid circles, experimental data by Peng *et al.* [35]; for other legends, see Fig. 2 caption.

and to the relativistic plane-wave Born cross sections calculated by Scofield [24]. Of the several nonexperimental cross sections presented in the figures, the present BEB-RBEB cross sections and the Born cross sections by Scofield are the only *ab initio* theories without any adjustable parameters.

Except for the carbon atom in Fig. 1, the relativistic cross sections begin to show a different shape than the shape of the nonrelativistic counterparts at $T>100$ keV. These figures clearly demonstrate the necessity for relativistic corrections for atoms with medium and high atomic numbers.

For the carbon atom, relativistic and nonrelativistic cross sections are almost identical for $T<1$ keV. Both the present RBEB cross section and the relativistic Quarles cross section marked as ''Quarles [20]'' are in good agreement with the experimental data by Tawara *et al.* [25], while the experimental data by Hink and Paschke [26] display an increasing

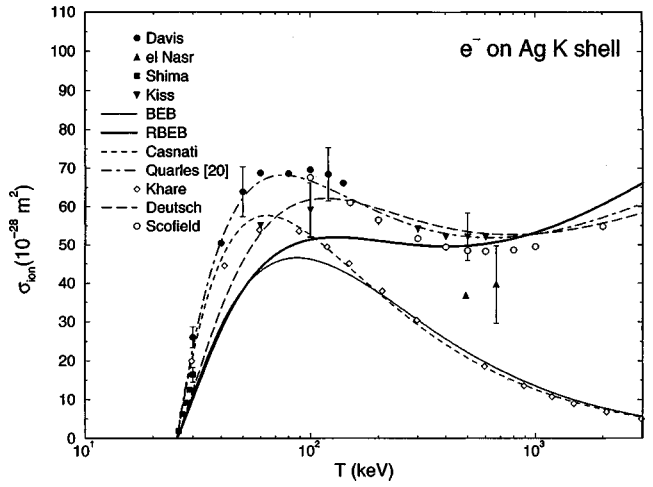

FIG. 5. *K*-shell ionization cross section of Ag. Circles, experimental data by Davis *et al.* [36]; upright triangles, data by el Nasr *et al.* [40]; squares, data by Shima *et al.* [37]; inverted triangles, data by Kiss *et al.* [38] cited in Long *et al.* [39]; for other legends, see Fig. 2 caption.

trend toward lower T not seen in any other theory or experiment.

For the argon atom in Fig. 2, all theoretical and experimental data seem to agree with each other, while our RBEB-BEB cross sections tend to agree slightly better with the experimental data by Tawara *et al.* [25], by Hippler *et al.* [27], and by Quarles and Semaan [28]. The experimental data by Platten *et al.* [29], though with large uncertainties, follow the shape of the Casnati cross section at low T. We also see the beginning of a trend that the relativistic Quarles and the nonrelativistic Casnati cross sections are higher than the RBEB-BEB cross sections in peak values. Although we did not extend Fig. 2 to very high incident electron energies, the relativistic plane-wave Born cross section by Scofield [24] is in excellent agreement with the present RBEB cross section to $T=10$ MeV.

For the nickel atom in Fig. 3, experiments and theories are both divided into two groups. The experimental data by Jessenberger and Hink [30] and the data by Luo *et al.* [31] agree with the peak values of the Quarles cross section and the nonrelativistic Khare cross section, while the experimental data by He *et al.* [32], the data by Pockman *et al.* [33] and the single data point by Smick and Kirkpatrick [34] are lower in peak values and agree with our RBEB-BEB cross sections. The relativistic plane-wave Born cross section by Scofield [24] rises rapidly near the peak overestimating the ionization cross section as expected. The present RBEB cross section begins to be higher than the plane-wave Born cross section beyond $T=1$ MeV. For H and He, the RBEB model produces M^2—the leading coefficient of the Bethe cross section in Eq. (23) as discussed in Sec. II D—higher than the known, reliable values [1]. Hence, we expect that the RBEB model would also overestimate M^2 for K shells of heavy atoms, resulting in a slightly higher cross section than the asymptotic Born cross section. A definitive experiment centered around the peak is desirable to distinguish different predictions from different theories.

In Fig. 4 we compare recent experimental data by Peng *et al.* [35] for the niobium atom to the present RBEB cross section, to the empirical formula by Casnati *et al.* [19] with the relativistic correction indicated by Quarles [20], and the semiempirical relativistic cross section by Deutsch *et al.* [22]. Here, the experimental data are in excellent agreement with the RBEB cross section, while the Casnati cross section is appreciably higher, reinforcing the trend also seen in Ar and Ni (Figs. 2 and 3).

Four sets of experimental data for the silver atom are compared to the present RBEB-BEB cross sections and other theories in Fig. 5. The experimental data by Davis *et al.* [36] agree well with the Quarles (= relativistic Casnati) cross section. The data by Davis *et al.* on the *K*-shell ionization of Cu and Au [36] are also much higher than our preliminary RBEB cross sections. The experimental data by Shima *et al.* [37] and by Kiss *et al.* [38]—as quoted in Long *et al.* [39]—lie in between the RBEB and the relativistic Quarles cross sections. The data by el Nasr *et al.* [40] disagree with all three relativistic cross sections presented in Fig. 5. Although all theoretical cross sections agree in the vicinity of $T=1$ MeV, the difference between the present RBEB cross section and the relativistic plane-wave Born cross section by Scofield [24] is widening at $T>2$ MeV, amplifying the trend observed in Ar and Ni, again due to the fact that the RBEB model is likely to overestimate M^2 in Eq. (23) for K electrons. The silver atom is another example for which definitive measurements near the peak would help to distinguish different theories.

B. Application of the relativistic BEQ cross section

Atomic hydrogen is a particularly simple case to apply Eq. (8) because only one nontrivial number is needed: $Q=0.5668$, which can be calculated exactly from the hydrogenic df/dw. The rest of the input data for the hydrogen atom are $B=13.6057$ eV, $u=U/B=1$ from the virial theorem, and $N=1$. As was shown in an earlier work [1], the nonrelativistic BEQ cross section is in excellent agreement with the experimental values measured by Shah *et al.* [41] from the threshold to $T=1$ keV. The relativistic BEQ cross section given by Eq. (21) is practically indistinguishable from the nonrelativistic BEQ cross section Eq. (8) from the threshold to $T\approx 5$ keV.

Since the ionization cross section is very low at relativistic T, the Fano plot is better suited for comparing different cross sections at relativistic T. The Fano plot is a graph using as the abscissa and ordinate

$$X=\ln\left(\frac{\beta_t^2}{1-\beta_t^2}\right)-\beta_t^2, \tag{38}$$

$$Y=\sigma\frac{\beta_t^2}{4\pi a_0^2\alpha^2}. \tag{39}$$

As can be seen from Eq. (23), such a plot will asymptotically approach a straight line with a slope M^2. Table II compares σ_{RBEB}, σ_{BEB}, and experimental data by Shah *et al.* [41] for the hydrogen atom at typical values of T and the corresponding X.

The experimental data for H by Shah *et al.* [41] are compared to the relativistic BEQ [Eq. (21)] and nonrelativistic BEQ [Eq. (8)] cross sections, and the asymptotic Bethe cross section [42] in a Fano plot in Fig. 6. We did not use the averaged cross sections, Eqs. (32)–(37), because they are meant for deep inner shells of many-electron atoms. Both the relativistic BEQ and the asymptotic Bethe cross sections agree with the experimental data within the experimental error bounds. However, the asymptotic Bethe cross section appears to agree better with the trend seen in the experimental data for $T>2$ keV than σ_{RBEQ}. This is an example in which the asymptotic Bethe cross section for the hydrogen atom is more accurate because exact wave functions are known. Although the actual cross-section values remain low at high T, the relativistic BEQ cross section is almost twice the nonrelativistic BEQ cross section at $T\approx 300$ keV (see Table II). Relativistic effects dominate at higher T, and the relativistic rise of the cross section occurs after $T\approx 1.5$ MeV.

TABLE II. Comparison of T, X [see Eq. (38)], σ_{RBEQ} [Eq. (21)], σ_{BEQ} [Eq. (8)], and experimental data by Shah *et al.* [41] for H.

T(keV)	X	σ_{RBEQ} (Å^2)	σ_{BEQ} (Å^2)	Expt. (Å^2)
0.998	−5.548	0.119	0.119	0.113±0.0077
1.998	−4.857	0.0663	0.0659	0.0631±0.0047
2.998	−4.454	0.0466	0.0462	0.0437±0.0036
3.998	−4.169	0.0362	0.0358	0.0339
5.0	−3.948	0.0297	0.0293	0.0279
10.0	−3.269	0.0161	0.0157	0.0149
50.0	−1.754	0.00409	0.00360	
100.0	−1.145	0.00243	0.00189	
300.0	−0.1851	0.00130	0.000681	
500.0	0.3251	0.00109	0.000422	
1000.0	1.161	0.000963	0.000221	
1500.0	1.738	0.000944	0.000151	
2000.0	2.183	0.000946	0.000115	
5000.0	3.756	0.000999	0.000048	
10000.0	5.048	0.00106	0.000025	

C. Application of the relativistic BED cross section

Recently, the nonrelativistic BED formula was applied to the helium atom in combination with the df/dw calculated from the relativistic random-phase approximation (RRPA) [43]. The resulting σ_{BED} was sufficiently accurate to be recommended as a normalization standard. In Ref. [43], the RRPA df/dw was fitted into a four-term power series to facilitate integration to an arbitrary upper limit in Eq. (6). The fitted equation is

$$df/dw = ay^3 + by^4 + cy^5 + dy^6, \tag{40}$$

where $y = B/E = B/(W+B)$, and $a = 8.24012$, $b = -10.4769$, $c = 3.964\,96$, and $d = -0.044\,597\,6$. To match the experimental threshold, $B = 24.587$ eV is used in Eq. (20) with $N = 2$ and a theoretical value of $U = 39.51$ eV for the helium atom [1].

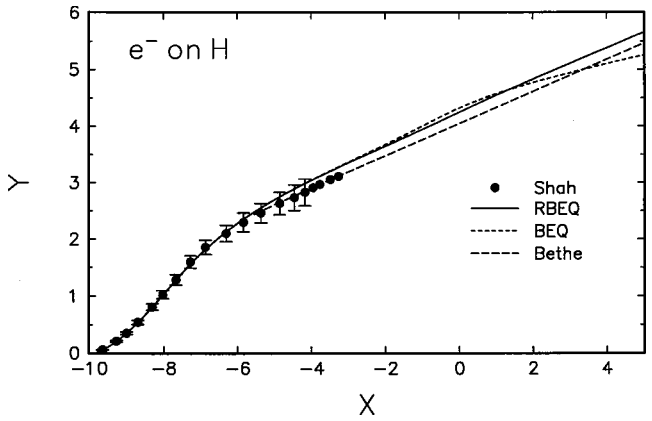

FIG. 6. Fano plot for H. The abscissa is given by Eq. (38) and the ordinate by Eq. (39). Solid curve, present relativistic RBEQ cross section Eq. (21); short-dashed curve, present nonrelativistic BEQ cross section Eq. (8); long-dashed curve, asymptotic Bethe cross section [42]; circles, experimental data by Shah *et al.* [41].

In Table III, σ_{RBED} and σ_{BED} are compared to the experimental data by Shah *et al.* [44] for the helium atom at typical values of T and the corresponding X. In Fig. 7, the experimental data for He by Shah *et al.* [44] and the data by Rieke and Prepejchal [45] are compared to the relativistic BED [Eq. (20)] and nonrelativistic BED [Eq. (5)] cross sections and the asymptotic Bethe cross section [42] in a Fano plot. As in the case of H, we did not use the averaged cross sections, Eqs. (32)–(37), for He because these equations are for deep inner shells of many-electron atoms. In contrast to the hydrogen atom, the RBED cross section represents the trend seen in the experimental data at $T > 5$ keV better than the asymptotic Bethe cross section.

Rieke and Prepejchal [45] presented their data as a fitted straight line using the variables for the Fano plot, Eqs. (38) and (39). They presented three pairs of constants for the ionization of the helium atom. Their experiment on He, however, represents the total inelastic scattering cross section that includes all discrete excitations because they used a buffer gas whose ionization energy is below the excitation energies of the metastable helium atom [46]. The excited He atoms produce buffer-gas ions through the Penning ionization. In Fig. 7 the error bars for the Rieke and Prepejchal curve represent the spread of the cross sections reproduced from the three sets of their constants, M^2 and C_R. All of their values are larger than the known asymptotic Bethe cross-section values for ionization.

As it was in the case of the hydrogen atom, σ_{RBED} [Eq. (20)] is almost twice the value of σ_{BED} [Eq. (5)] at $T \approx 300$ keV, and then the former dominates for higher T (see Table III). The relativistic rise of σ_{RBED} again occurs after $T \approx 1.5$ MeV.

D. BEB cross section for xenon

The BEB model requires minimal input data for the target atom and hence the model is most useful for atoms with

TABLE III. Comparison of T, X [see Eq. (38)], σ_{RBED} [Eq. (20)], σ_{BED} [Eq. (5)], and experimental data by Shah *et al.* [44] for He.

T(keV)	X	σ_{RBED} (Å^2)	σ_{BED} (Å^2)	Expt. (Å^2)
1.0	−5.546	0.137	0.137	0.128 ±0.0079
2.01	−4.851	0.0803	0.0799	0.0796±0.0049
3.0	−4.453	0.0580	0.0576	0.0551±0.0034
4.0	−4.168	0.0458	0.0453	0.0448±0.0028
6.1	−3.752	0.0321	0.0316	0.0308±0.0019
8.0	−3.487	0.0256	0.0250	0.0250±0.0015
10.0	−3.269	0.0212	0.0206	0.0195±0.0012
50.0	−1.754	0.00561	0.00494	
100.0	−1.145	0.00337	0.00264	
300.0	−0.1851	0.00183	0.000969	
500.0	0.3251	0.00155	0.000606	
1000.0	1.161	0.00139	0.000320	
1500.0	1.738	0.00138	0.000220	
2000.0	2.183	0.00139	0.000168	
5000.0	3.756	0.00149	0.000072	
10000.0	5.048	0.00161	0.000038	

complex structure. Xenon is a good example because its total ionization cross section is known to a reasonable accuracy ($\pm 10\%$–15%) at $T \leqslant 5$ keV [47–49] and $T = 0.1$–2.7 MeV [45]. One complication common in heavy atoms such as xenon is the fact that multiple ionization is a significant fraction of the total ionization cross section. For instance, Wetzel *et al.* [47] and Nagy *et al.* [48] separately measured cross sections for producing singly charged, doubly charged, and triply charged ions, while Nishimura and Sakae [49] measured the total ion current. A simple sum of the cross sections measured by Wetzel *et al.* or Nagy *et al.* is known as the counting ionization cross section defined by

$$\sigma_{count} = \sum \sigma^{n+}, \quad n = 1,2,3, \ldots, \tag{41}$$

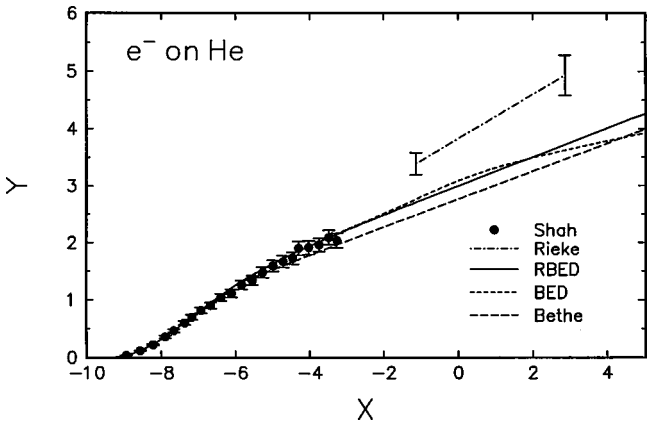

FIG. 7. Fano plot for He. Solid curve, present relativistic RBED cross section, Eq. (20); short-dashed curve, present nonrelativistic BED cross section, Eq. (5); long-dashed curve, asymptotic Bethe cross section [42]; dot-dashed curve, experimental data by Rieke and Prepejchal [45], see text for the explanation of the error bounds; circles, experimental data by Shah *et al.* [44].

while the ion current measured by Nishimura and Sakae is known as the gross ionization cross section defined by

$$\sigma_{gross} = \sum n\sigma^{n+}, \quad n = 1,2,3, \ldots. \tag{42}$$

Most of the multiply charged ions result from the Auger process triggered by the ionization of an inner shell, such as the $4s$, $4p$, $4d$, and $5s$ orbitals. Holes created in very deep inner shells are more likely to be filled by fluorescence than by the Auger process. Besides, ionization cross sections for the K, L, and M shells are negligible compared to cross sections of the outer shells, and we need to consider multiple ionization from the holes created only in the N shell and O shell.

Since our theoretical model is simple and the accuracy of the available experimental ionization cross sections is modest, it is not necessary for us to know the details of the Auger process, such as fluorescence yields and partial cross sections for the numerous channels of Auger decay. It is sufficient for us to consider only the energy balance from the list of orbital binding energies in Table IV. For instance, the ionization of a $5s$ electron will lead to a doubly charged ion when a $5p$ electron fills the $5s$ hole, while the ionization of a $4d$ electron will lead to a triply charged ion by first filling the $4d$ hole by a $5s$ electron and then the resulting $5s$ hole filled by a $5p$ electron. In reality it is also possible to get only a doubly charged ion if a $5p$ electron fills the $4d$ hole. Similarly, we assume that the ionization of a $4s$ or $4p$ electron will result in a quadruply charged ion. It is easy to estimate the cross sections for the production of these multiply charged ions in the BEB model because the model gives cross sections for each orbital. Hence, to get the counting ionization cross section, we simply add each orbital cross section once. For the gross ionization cross section we double the $5s$ cross section, triple the $4d$ cross section, and

TABLE IV. Orbital binding energy B, kinetic energy U, electron occupation number N, and the Bethe constants M^2 [Eq. (30)], C_{NR} [Eq. (31)], and C_R [Eq. (25)] for Xe. N, C_{NR}, and C_R are dimensionless. The lowest binding energy is experimental. For other binding energies, we used the orbital energies from the Dirac-Fock wave function.

Orbital	B (eV)	U (eV)	N	$M^2(a_0^2)$	C_{NR}	C_R
$1s_{1/2}$	35755.82	42281.58	2	0.000391	−0.00229	0.001564
$2s_{1/2}$	5509.33	9173.91	2	0.002470	−0.00989	0.01441
$2p_{1/2}$	5161.43	9135.67	2	0.002636	−0.01038	0.01556
$2p_{3/2}$	4835.57	8324.23	4	0.005627	−0.02180	0.03358
$3s_{1/2}$	1170.37	2722.32	2	0.01163	−0.02853	0.08586
$3p_{1/2}$	1024.78	2642.38	2	0.01328	−0.03083	0.09983
$3p_{3/2}$	961.25	2453.45	4	0.02831	−0.06391	0.2147
$3d_{3/2}$	708.13	2311.18	4	0.03843	−0.07502	0.3031
$3d_{5/2}$	694.90	2261.96	6	0.05874	−0.1136	0.4645
$4s_{1/2}$	229.39	757.48	2	0.05931	−0.04893	0.5347
$4p_{1/2}$	175.58	690.54	2	0.07749	−0.04321	0.7193
$4p_{3/2}$	162.80	643.34	4	0.1671	−0.08057	1.564
$4d_{3/2}$	73.78	497.77	4	0.3688	0.1141	3.744
$4d_{5/2}$	71.67	485.43	6	0.5695	0.1928	5.797
$5s_{1/2}$	27.49	122.58	2	0.4950	0.6419	5.513
$5p_{1/2}$	13.40	88.90	2	1.015	2.045	12.03
$5p_{3/2}$	12.1298	79.42	4	2.243	4.744	26.82

quadruple the $4s$ and $4p$ cross sections. The values of B and U given in Table IV for xenon were calculated using a single-configuration Dirac-Fock wave function.

The BEB cross section for the gross ionization is compared to available experiments at low T in Fig. 8, while the Fano plot for Xe is shown in Fig. 9 for relativistic T. The BEB cross section used in Fig. 8 is σ_{BEBav} [Eq. (34)], while the cross section used in Fig. 9 is σ_{RBEBav} [Eq. (37)]. The relativistic and nonrelativistic BEB cross sections are indistinguishable at nonrelativistic T. For the $5p_{1/2}$ and $5p_{3/2}$ orbitals, we did not use the ''average'' cross section in Eq. (34). Instead we replaced $u+1$ in Eq. (11) by $(u+1)/n$ with the principal quantum number $n=5$ as we did in earlier applications of the BEB model to heavy atoms and molecules containing heavy atoms. This is another example of the fine tuning of the ''Burgess'' denominator to avoid excessive reduction of cross sections due to large values of U for outer orbitals resulting from many radial nodes and high angular quantum numbers in the kinetic energy operator $\hbar(l+1)/2r^2$. Except for the outermost orbitals, such as the $5p_{1/2}$ and $5p_{3/2}$ orbitals, the averaging of two denominators shown in Eq. (34) leads to cross sections practically indistinguishable from those obtained by using $(u+1)/n$ in the denomi-

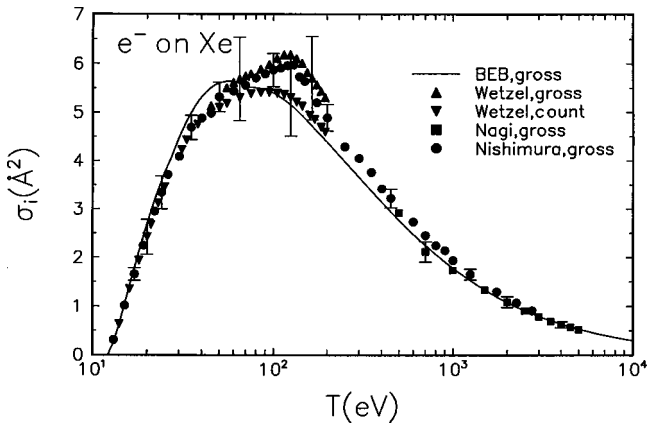

FIG. 8. Total ionization cross section of Xe. Solid curve, present BEB gross ionization cross section, Eq. (34); upright triangles, experimental gross ionization cross section by Wetzel *et al.* [47]; inverted triangles, experimental counting ionization cross section by Wetzel *et al.* [47]; squares, experimental gross ionization cross section by Nagy *et al.* [48]; circles, experimental gross ionization cross section by Nishimura and Sakae [49].

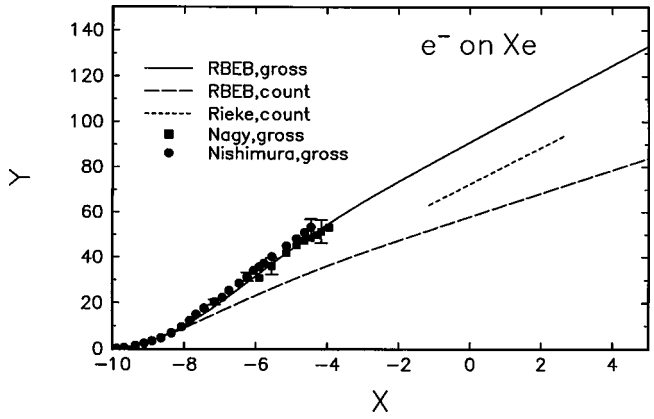

FIG. 9. Fano plot for Xe. Solid curve, present RBEB gross ionization cross section Eq. (37); long-dashed curve, present RBEB counting ionization cross section; short-dashed curve, experimental counting ionization cross section by Rieke and Prepejchal [45]; squares, experimental gross ionization cross section by Nagy *et al.* [48]; triangles, experimental counting ionization cross section by Nagy *et al.* [48]; circles, experimental gross ionization cross section by Nishimura and Sakae [49].

nator. An alternative method is to use the orbital kinetic energies derived from an effective core potential, which generates nodeless valence orbitals. Effective core potentials are widely used in quantum chemistry for molecules containing heavy atoms [50]. We also used experimental ionization energy for the outermost orbital to match the threshold of experimental cross sections.

In the case of He, double ionization is negligible and we did not have to distinguish counting and gross ionization cross sections. For Xe, however, the gross ionization cross section is visibly higher than the counting ionization cross section as can be seen from Figs. 8 and 9. The peak near $T=110$ eV is enhanced in the gross ionization cross section, a clear indication that the peak is related to the multiple ionization resulting from holes in the $4d_{3/2}$ and $4d_{5/2}$ orbitals. These holes may be created either by direct ionization or excitation to a higher bound levels, which decay by autoionization. The BEB model includes the direct ionization but not the autoionizing excitations. Within the context of the BEB model, the autoionization cross sections must be calculated separately and added on to the direct ionization cross section.

For heavy, neutral atoms, the BEB model underestimates the value of M^2 while overestimating C_{NR} and consequently C_R. The BEB values for Xe are $M^2=5.157$, $C_{NR}=7.209$, and $C_R=57.96$ for the counting ionization cross section, and $M^2=8.441$, $C_{NR}=7.947$, and $C_R=91.01$ for the gross ionization cross section. Rieke and Prepejchal [45] detected Xe ions in the Geiger-Müller (GM) counting mode, and hence what their instrument recorded corresponds to the counting ionization cross section. In spite of the low uncertainty estimate on their total M^2 value, 8.04 ± 0.15, their value far exceeds the $M^2=6.12$ obtained by Berkowitz [14] directly from photoionization data. The value by Rieke and Prepejchal quoted above was obtained without any buffer gas in the counter, which implies that there was no conversion of metastable Xe into an ion through the Penning ionization. Hence their value of $M^2=8.04\pm0.15$ and $C_R=72.35\pm0.40$ should be for ionization without any excitations unlike the case of He. In fact, this tendency of the M^2 values determined by Rieke and Prepejchal being higher than the M^2 values obtained directly from photoionization is seen in many targets reported by Rieke and Prepejchal. We have no plausible explanation for this trend.

IV. CONCLUSIONS

The nonrelativistic BED, BEQ, and BEB cross sections for electron-impact ionization have been extended to relativistic incident electron energies. The original BED-BEQ-BEB formulas, which reproduce reliable ionization cross sections for neutral targets, have been modified slightly for applications to inner shells by using a simple average of cross sections with two different denominators. These denominators play the role of T-dependent scaling of ionization cross section to account for the electron correlation between the incident and target electrons. The relativistic formulas can now be used for the ionization of atoms and molecules whose inner-shell ionization requires relativistic ($T>20$ keV) incident electron energies.

The present theory is in excellent agreement with available experimental data on K-shell ionization by Tawara *et al.* [25] for carbon and argon, the experimental data by Pockman *et al.* [33] for nickel, and with the experimental data by Peng *et al.* [35] for niobium. The present theory is lower than available experimental data for silver. For nickel and heavier elements, the relativistic version of the empirical Casnati cross sections tends to be higher than the present theory at the peak by 20% to 30%. Definitive experiments for the K-shell ionization of Ni and Ag near the cross-section peaks are needed to settle conflicting theories and experiments.

The present theory is also in good agreement with the relativistic plane-wave Born cross sections by Scofield [24] for argon, nickel, and silver for $T<2$ MeV. However, for higher T, the RBEB cross section is higher than the Born cross section, because the RBEB model most likely overestimates M^2 [Eq. (23)] for K shells. This shortcoming of the RBEB model can be corrected by actually calculating M^2 with a suitable relativistic continuum wave function. Since the ionization energy for K electrons is high and the bound state is dominated by the nuclear Coulomb field, electron correlation is not expected to be critical. Any reasonable continuum wave-function model—e.g., a relativistic version of the Hartree-Fock continuum wave function with frozen core orbitals—is likely to produce M^2 values better than the simple form, Eq. (30), used in the RBEB model. When such continuum wave functions become available, the RBEQ and RBED models can be used as well.

Although the empirical equation by Casnati *et al*. [19] has a logarithmic term to represent the dipole interaction, its relativistic correction derived by Quarles [20] is based on the classical theory by Gryzinski [21], which does not have the proper dipole interaction term. Hence, it is uncertain whether this combination of nonrelativistic Casnati formula and the Quarles relativistic correction would necessarily lead to the correct asymptotic behavior for the dipole interaction, which becomes dominant at relativistic T. The same comment applies to the relativistic extension of the semiempirical cross section by Deutsch *et al.* [22]. The Deutsch cross section does not have the correct logarithmic term for the dipole interaction either in the relativistic or the nonrelativistic formula. It is known that the lack of a proper dipole interaction term in the classical theory leads to cross sections too low at high T.

All forms of the present theory and the plane-wave Born cross section by Scofield [24] have the correct logarithmic terms for the dipole interaction. In Figs. 3–5, the RBEB cross section becomes higher than the semiempirical cross sections marked ''Quarles [20]'' and ''Deutsch'' at $T>2$ MeV. Since these semiempirical cross sections both have ''improper'' asymptotic behavior, the only meaningful comparison of asymptotic cross sections will be the comparison between the present theory and the plane-wave Born cross section by Scofield [24].

The Born approximation overestimates peak cross sections and this expectation is borne out by the trend seen in Fig. 3. The agreement near the peak in Fig. 5 between the

Born cross section by Scofield and the experimental data by Davis *et al.* [36] should be regarded not as an agreement but as an indication that the data by Davis *et al.* are too high in view of the expected behavior of Born cross sections near the peak. The comparison of the present σ_{RBEB} to the Born cross section by Scofield at $T=10$ MeV for medium to heavy atoms indicates that the former is higher than the latter by 10–15%.

The ionization cross sections for the hydrogen and helium atoms are in excellent agreement with the present BEQ/BED cross sections at nonrelativistic T. However, the asymptotic trend of the experimental data for the hydrogen atom follows the asymptotic Bethe cross section [42] better than the relativistic BEQ cross section. On the other hand, the asymptotic trend of the experimental data for the helium atom follows the relativistic BED cross section.

The BEB cross section for Xe is in good agreement with available experiments except near the cross-section peak, where autoionization resulting from the ''excitations'' of the $5s$ and $4d$ electrons to upper bound levels interact with the background continuum for the direct ionization of the $5p$ electrons. The BEB model does not include these autoionizing channels, though the model can approximately account for the multiple ionization produced by the Auger decay of the $5s$, $4d$, $4p$, and $4s$ holes created by direct ionization.

When accurate data on differential dipole oscillator strength are available, the BED and BEQ models will lead to the correct value of the leading dipole term M^2 in the asymptotic Bethe cross section [see Eq. (23)] for relativistic incident electron energies. However, the present theory is likely to overestimate the second term C_R in the asymptotic Bethe cross section. Hence the BED and BEQ models may still overestimate counting ionization cross sections for extreme relativistic incident electron energies, $T \gg mc^2$. For gross ionization cross sections, available experimental data are insufficient to draw any definite conclusion about the reliability of the present theory at $T \gg mc^2$, though the BED and BEQ cross sections are also likely to overestimate gross ionization cross sections at $T \gg mc^2$.

Unlike K shells, the BEB model underestimates M^2 of heavy neutral atoms and overestimates their C_R and C_{NR}. The fact that the BEB model produces reliable ionization cross sections at low T for many neutral atoms and molecules indicates that other terms in the BEB-RBEB model compensate at low T.

The underlying reasons for the surprising success of the Burgess denominator for neutral targets and its modified form for inner shells presented here are not clear at present. More application examples are needed to fully understand the fundamental nature of the Burgess denominator. Only then the BED-BEQ-BEB models can be modified further to make them truly versatile models that not only cover the entire range of T but also apply to neutral as well as ionized targets.

Since all the input data required in the relativistic BEB cross section can be obtained from the ground-state wave function (preferably Dirac-Fock type) of a target atom, σ_{RBEB} [Eqs. (22) or (37)] can be used for a wide range of neutral atoms and molecules as well as atomic and molecular ions. The relativistic formulas presented in this paper provide a ''seamless'' coverage of ionization cross sections from the threshold to relativistic incident energies, making the formulas ideally suited for modeling of radiation effects, fusion plasmas, stripping of ions in heavy ion fusion, inner-shell ionization, and other applications where ionization cross sections for a wide range of incident energies are required.

ACKNOWLEDGMENTS

This work was supported in part by the Office of Fusion Energy Sciences, U.S. Department of Energy and by FCT (Portugal) under Project No. PRAXIS/C/FIS/10030/98. Y.K.K and J.P.S are also grateful for support from the Luso-American Development Foundation.

[1] Y.-K. Kim and M.E. Rudd, Phys. Rev. A **50**, 3954 (1994).
[2] N.F. Mott, Proc. R. Soc. London, Ser. A **126**, 259 (1930).
[3] L.D. Landau and E.M. Lifshitz, *Quantum Mechanics: Nonrelativistic Theory*, 2nd ed. (Pergamon, London, 1965), p. 575, Eq. (145.17).
[4] H. Bethe, Ann. Phys. (Leipzig) **5**, 325 (1930).
[5] C. Møller, Ann. Phys. (Leipzig) **14**, 531 (1932).
[6] Applications of the BED/BEB model to many atoms and molecules and relevant references can be found at *http://physics.nist.gov/ionxsec*.
[7] M. Inokuti, Rev. Mod. Phys. **43**, 297 (1971).
[8] D.S. Soh, B.H. Cho, and Y.-K. Kim, Phys. Rev. A **26**, 1357 (1982).
[9] A. Burgess, *Proceedings of the 3rd International Conference on Electronic and Atomic Collisions, London, 1963*, edited by M.R.C. McDowell (North-Holland, Amsterdam, 1964), p. 237; Proceedings of the Symposium on Atomic Collision Processes in Plasmas, Culham, 1964 [AERE Report No. 4818], p. 63.
[10] Y.-K. Kim, Radiat. Res. **64**, 205 (1975), Eqs. (A1) and (A2).
[11] H. Bethe, Z. Phys. **76**, 293 (1932); in *Handbuck der Physik*, edited by H. Geiger and K. Scheel (Springer, Berlin, 1933), Vol. 24/1, p. 273.
[12] H.A. Bethe and J. Ashkin, in *Experimental Nuclear Physics*, edited by E. Segrè (Wiley, New York, 1953), Vol. 1, p. 166, Eq. (71).
[13] U. Fano, Phys. Rev. **95**, 1198 (1954); **102**, 385 (1956); Annu. Rev. Nucl. Sci. **13**, 1 (1963).
[14] J. Berkowitz, *Photoabsorption, Photoionization, and Photoelectron Spectroscopy* (Academic Press, New York, 1979), Chap. V.
[15] Y.-K. Kim, K.K. Irikura, and M.A. Ali, J. Res. Natl. Inst. Stand. Technol. **105**, 285 (2000).
[16] S.M. Younger, J. Quant. Spectrosc. Radiat. Transfer **26**, 329 (1981).
[17] C.J. Powell, in *Electron Impact Ionization*, edited by T.D. Märk and G.H. Dunn (Springer-Verlag, Vienna, 1985), Chap.

6; C.J. Powell, in *Microbeam Analysis—1990*, edited by J.R. Michael and P. Ingram (San Francisco Press, San Francisco, 1990), p. 13.
[18] R.D. Deslattes, E.G. Kessler, Jr., P. Indelicato, and E. Lindroth, in *International Tables for Crystallography*, edited by A.J.C. Wilson and E. Prince (Kluwer Academic Publishers, Boston, 1999), Vol. C, Chap. 4.2.2, pp. 200–213, Table 4.4.2.4.
[19] E. Casnati, A. Tartari, and C. Baraldi, J. Phys. B **15**, 155 (1982).
[20] C.A. Quarles, Phys. Rev. A **13**, 1278 (1976).
[21] M. Gryzinski, Phys. Rev. **138**, A305 (1965); **138**, A322 (1965); **138**, A336 (1965).
[22] H. Deutsch, K. Becker, and T.D. Märk, Int. J. Mass Spectrom. **177**, 47 (1998).
[23] S.P. Khare, V. Saksena, and J.M. Wadehra, Phys. Rev. A **48**, 1209 (1993).
[24] J.H. Scofield, Phys. Rev. A **18**, 963 (1978).
[25] H. Tawara, K.G. Harrison, and F.J.D. Heer, Physica (Amsterdam) **63**, 351 (1973).
[26] W. Hink and H. Paschke, Z. Phys. **244**, 140 (1971).
[27] R. Hippler, K. Saeed, I. McGregor, and H. Kleinpoppen, Z. Phys. A **307**, 83 (1982).
[28] C. Quarles and M. Semaan, Phys. Rev. A **26**, 3147 (1982).
[29] H. Platten, G. Schiwietz, and G. Nolte, Phys. Lett. **107A**, 89 (1985).
[30] J. Jessenberger and W. Hink, Z. Phys. A **275**, 331 (1975).
[31] Z. Luo, Z. An, F. He, T. Li, X. Long, and X. Peng, J. Phys. B **29**, 4001 (1996).
[32] F.Q. He, X.F. Peng, X.G. Long, Z.M. Luo, and Z. An, Nucl. Instrum. Methods Phys. Res. B **129**, 445 (1997).
[33] L.T. Pockman, D.L. Webster, P. Kirkpatrick, and K. Harworth, Phys. Rev. **71**, 330 (1947).
[34] A.E. Smick and P. Kirkpatrick, Phys. Rev. **67**, 153 (1945).
[35] X. Peng, F. He, X. Long, Z. Luo, and Z. An, Phys. Rev. A **58**, 2034 (1998).
[36] D.V. Davis, V.D. Mistry, and C.A. Quarles, Phys. Lett. **38A**, 169 (1972).
[37] K. Shima, T. Nakagawa, K. Umetani, and T. Mikumo, Phys. Rev. A **24**, 72 (1981).
[38] K. Kiss, Gy. Kálmán, J. Pálinkaás, and B. Schlenk, Acta Phys. Acad. Sci. Hung. **50**, 97 (1981).
[39] X. Long, M. Lin, F. Ro, and X. Peng, At. Data Nucl. Data Tables **45**, 353 (1990).
[40] S.A.H.S. el Nasr, D. Berenyi, and G. Bibok, Z. Phys. **267**, 169 (1974).
[41] M.B. Shah, D.S. Elliott, and H.B. Golbody, J. Phys. B **20**, 3501 (1987); and private communication.
[42] Y.-K. Kim and M. Inokuti, Phys. Rev. A **3**, 665 (1971).
[43] Y.-K. Kim, W.R. Johnson, and M.E. Rudd, Phys. Rev. A **61**, 034702 (2000).
[44] M.B. Shah, D.S. Elliott, P. McCallion, and H.B. Gilbody, J. Phys. B **21**, 2751 (1988).
[45] F.F. Rieke and W. Prepejchal, Phys. Rev. A **6**, 1507 (1972).
[46] M. Inokuti, Y.-K. Kim, and R.L. Platzman, Phys. Rev. **164**, 55 (1967).
[47] R.C. Wetzel, A. Baiocchi, T.R. Hays, and R.S. Freund, Phys. Rev. A **35**, 559 (1987).
[48] P. Nagy, A. Skutlartz, and V. Schmidt, J. Phys. B **13**, 1249 (1980).
[49] H. Nishimura and T. Sakae (private communication).
[50] W.M. Huo and Y.-K. Kim, Chem. Phys. Lett. **319**, 576 (2000).